

We are IntechOpen, the world's leading publisher of Open Access books Built by scientists, for scientists

6,900

Open access books available

186,000

International authors and editors

200M

Downloads

Our authors are among the

154

Countries delivered to

TOP 1%

most cited scientists

12.2%

Contributors from top 500 universities



WEB OF SCIENCE™

Selection of our books indexed in the Book Citation Index
in Web of Science™ Core Collection (BKCI)

Interested in publishing with us?
Contact book.department@intechopen.com

Numbers displayed above are based on latest data collected.
For more information visit www.intechopen.com



Using Numerical Methods to Design and Control Heating Induction Systems

Julio Walter and Gerardo Ceglia
Universidad Simón Bolívar
 Venezuela

1. Introduction

Although induction heating systems exist since 1906 (Curtis, 1950) its design always has been an art, with a great emphasis in the designer's experience. This state of things has not really changed much until the advent of computers and analysis software powerful enough. Now it is possible to use relatively common programs, even free software in some cases, to design and simulate the heating system before any physical device needs to be mounted. This chapter is devoted to show some of these techniques and to present examples that illustrates it.

2. Modeling of the heating coil and load.

2.1 The transformer effect

The principle involved in transferring energy from a heating inductor to a load is equivalent to a transformer which primary and secondary are composed by the induction coil and the load, respectively. This can be better seen in Fig. 1, where an alternating current applied to the heating coil induces another current into the load which may be modeled as a single loop inductance with a series resistance formed by the outside ring (dotted region) of the load. This ring is forced by the Skin Effect (Marion, 1980) that coerces the current to flow in a shell which geometry is dependant from various parameters (frequency, conductivity, dimensions, topology, etc).

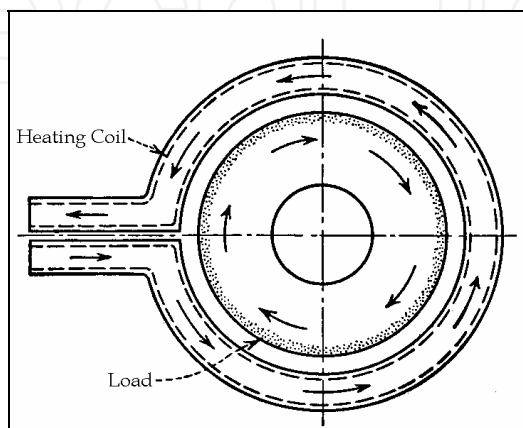


Fig. 1. Current distribution in an induction heating system

The shell formed by the Skin Effect is the main influence that determine load's inductance and resistance and they should be calculated using a Magnetic Finite Element program since they are too complex (or perhaps impossible) to evaluate in an analytical way, except for the most simplest cases which has academic interest only.

The coil-load system represented in the figure 2A shows a standard heating system viewed in the sense of the current flow. Its electrical equivalent can be seen in Fig. 2B, where L_p and L_s are, respectively, the coil and the load self inductances; M represents the mutual inductance between L_p and L_s while R_s is the real part of the load resistance and V_1 , V_2 , I_1 and I_2 are the system voltages and currents.

2.2 Mathematical representation of the heating system

Using the Kirchoff Voltage Law it is possible to set the equations (1) and (2) which describes mathematically the model derived from the circuit shown in Fig. 2B.

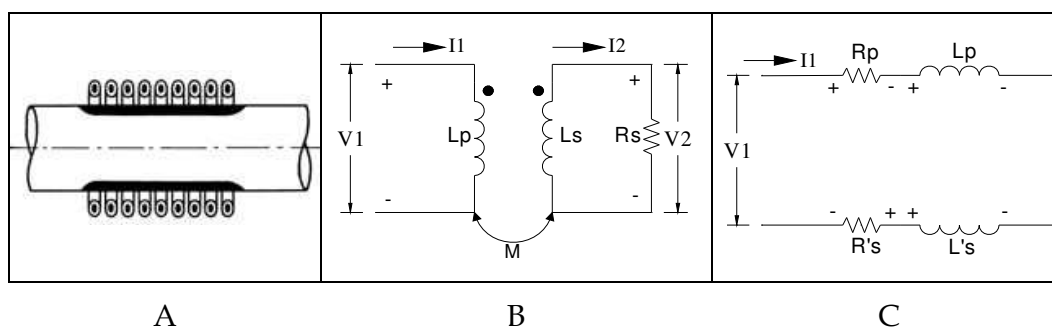


Fig. 2. A: Coil-Load system, B: Electrical Equivalent, C: Electrical Reduced Equivalent

$$V_1 = j\omega L_p I_1 - j\omega M I_2 \quad (1)$$

$$-V_2 = -j\omega M I_1 + j\omega L_s I_2 \quad (2)$$

Taking in consideration the dot standard, it is possible to write I_2 in function of I_1 , as follows

$$I_2 = \frac{j\omega M}{R_s + j\omega L_s} I_1 \quad \text{where } R_s = \frac{V_2}{I_2} \quad (3)$$

Using (3) to eliminate I_2 from (1),

$$V_1 = \left[j\omega L_p + \frac{\omega^2 M^2}{R_s + j\omega L_s} \right] I_1 \quad (4)$$

Equation (4) has an interesting implication. It suggests that the impedance $Z = V_1/I_1$ seen from the primary side is equivalent to a single non coupled inductor of L_p Henrys serially connected with an additional impedance. Expanding this second term:

$$Z_R(j\omega) = \frac{\omega^2 M^2}{R_s + j\omega L_s} = \frac{\omega^2 M^2}{R_s + j\omega L_s} \cdot \frac{R_s - j\omega L_s}{R_s - j\omega L_s} = \frac{R_s \omega^2 M^2}{R_s^2 + \omega^2 L_s^2} - \frac{j\omega^3 L_s M^2}{R_s^2 + \omega^2 L_s^2} \quad (5)$$

Rewriting equation (5)

$$Z_R(j\omega) = \frac{R_s \omega^2 M^2}{R_s^2 + \omega^2 L_s^2} - j\omega \left(\frac{\omega L_s M^2}{R_s^2 + \omega^2 L_s^2} \right) = R'_s + j\omega(-L'_s) \quad (6)$$

The first term of equation (6) is the impedance's real part and it corresponds to the ohmic resistance of the load reflected to the primary side of the induction heating coil. The second term reflects as negative impedance that reduces the total system's inductance.

The circuit that represents the total heating system is shown in Fig. 2C, where R_p and L_p again represents the primary's coil resistance and self inductance, R'_s and L'_s are the values of R_s and L_s reflected to the primary side by equation (5).

3. Heating coil design using finite element magnetic software

Having deduced the mathematical relationship between the heating coil and the load, it is necessary now to obtain the parameters needed to feed this model. These parameters are induction coil inductance (L_p) and resistance (R_p), load inductance (L_s) and resistance (R_s) and its mutual inductance. These parameters plus the working frequency, which is an external variable, permit to evaluate completely the impedance of the heating coil-load system.

3.1 Finite Elements Methods Magnetics software (FEMM)

Although there are several Finite Elements Methods Magnetics programs in the market (www.comsol.com), Visimag (www.vizimag.com), etc., we chose FEMM (www.femm.info) because is powerful enough and is free software. It limits the simulations to only 2 dimensions, but most of the heating coils have some degree of symmetry that permits accurate results using 2D analysis. An in deep examination of the FEMM software is beyond the purpose of this book but we encourage to the reader that he or she review extensively the tutorials and documentation to gain know-how in the area, there is also some terminology which is not defined here but it is in the FEMM user's manual (Meeker, 2009).

Although FEMM is capable of giving the total inductance and resistance for the associated system, it is necessary to obtain independently the primary resistance (R_p) and the load resistance (R'_s), because the first is associated with losses in the induction coil and it is quite recommendable to minimize it. On the contrary, the second is associated with the energy transfer to the load and should be maximized.

Having both R_p and R'_s it is possible to define an important parameter, the heating efficiency of the system. Since the flowing current is the same for both (see Fig. 2C):

$$\eta_{heat} = \frac{W_{LOAD}}{W_{Total}} \cdot 100\% = \frac{I^2 \cdot R'_s}{I^2 \cdot R'_s + I^2 \cdot R_p} \cdot 100\% = \frac{R'_s}{R'_s + R_p} \cdot 100\% \quad (7)$$

The associated resistances are evaluated within the FEMM postprocessor as we shall study in the next paragraph.

3.2 Defining the structure of the induction coil and load system

To obtain the needed parameters it is necessary first to define the geometry of the heating system and the material to be heated; the material used to make the heating coil is always copper, so it is already predetermined. Once the geometry is defined, it is necessary to draw

it on the FEMM user's interface or, better, in a CAD (Computer Aided Design) program capable of export the draw in DXF (Drawing Exchange File) format which will be then imported in FEMM. This last approach is very useful because the FEMM user's interface lack some drawing facilities that are included in other CAD programs, like AutoCAD®.

The next step, once in FEMM, is defining the materials, boundaries and other properties required to run the finite element algorithm (see the FEMM tutorials and manual). The postprocessor has the facilities to extract the values needed to calculate the parameters mentioned before. To clarify the entire simulation process, it will be shown a working example.

3.3 Working example: Design of a small aluminum melting furnace

3.3.1 Initials definitions

It is required to design a furnace to melt approximately 0,5 kg of aluminum. The crucible is given and is shown in the figure 3A. Since the crucible has symmetry on its axis, the magnetic problem reduces to an axisymmetric 2D system; figure 3B shows the transversal cutting for the internal side of the crucible, where the metal will be melted. In this case the crucible is formed by a nonconductive material, so it will not be taking into account for the finite element calculation.

For the axisymmetric problem is necessary only to define half of the transversal cutting, as the FEMM program determine the contribution of the 2D slice and calculate then the total produced by the corresponding solid of revolution. Figure 4A shows this draw made in AutoCAD® which includes also the heating coil; figure 4B shows the system already imported in FEMM. The measurements units in the CAD should be defined either in millimeters, centimeters, meters or inches since these dimensions will be exported to FEMM via DXF and is information relevant to the program. Now it is required to define all the regions with its corresponding materials. No region could be left undefined; in case the user needs to leave out some regions, it must be defined as "no mesh" as showed in Figure 4C where these definitions supports the working problem.

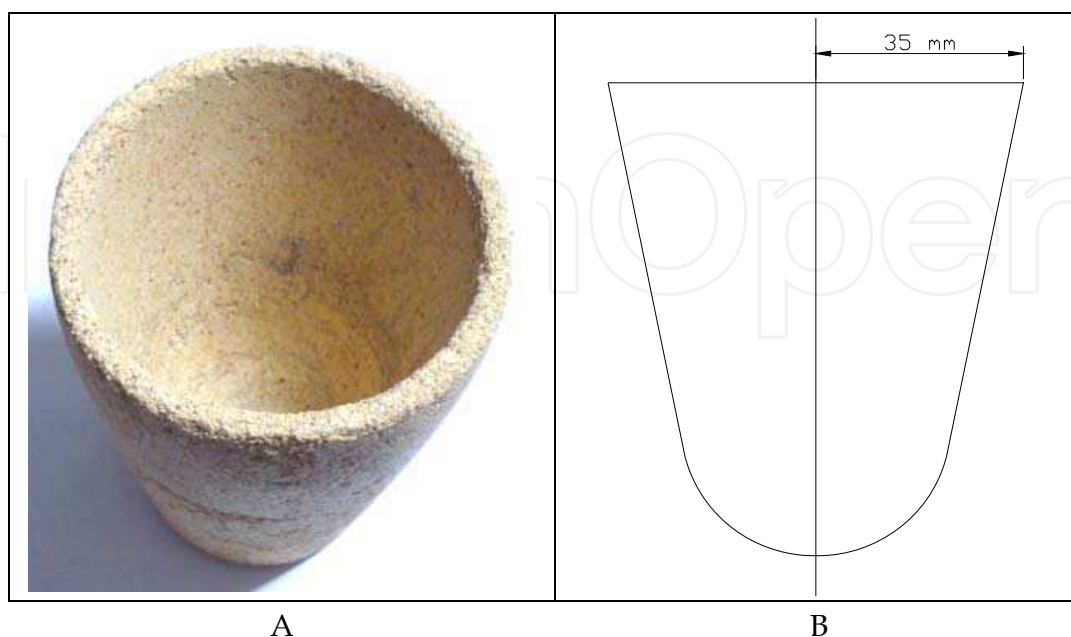


Fig. 3. A: Crucible, B: Internal crucible transversal cutting

It is necessary to point out that all the turns of the heating coil has to be defined as a “circuit” in FEMM to accomplish correctly the simulation (see “circuits” in FEMM manual). In the working example this circuit was named “HeatingCoil” and it is necessary also to apply to the circuit a current different from zero, which, for this example, was chosen as 100 amperes.

3.3.2 Simulation

Simulation requires having some knowledge of the final working frequency. There are various ways to estimate it but one of the easiest method is using tables or graphics of the penetrations deep (δ) against frequency. Figure 5 (Martínez & Esteve, 2003) shown one example of this, where is possible to obtain δ for several common materials and frequencies. To prevent current cancelation inside the load and thus maximize the power transfer within it, a simple rule of thumb state that the radius of the piece to be heated has to be greater than 10 times the penetration deep, so if the load has a radius of 35 mm, δ must be less than 3,5 mm. Locating this region in fig. 5 and searching the intersection with the material used (aluminum at 500 °C) it is possible to obtain an adequate frequency range to operate the system. A frequency of 40 kHz and a 0,5 mm deep are good estimates for this study case.

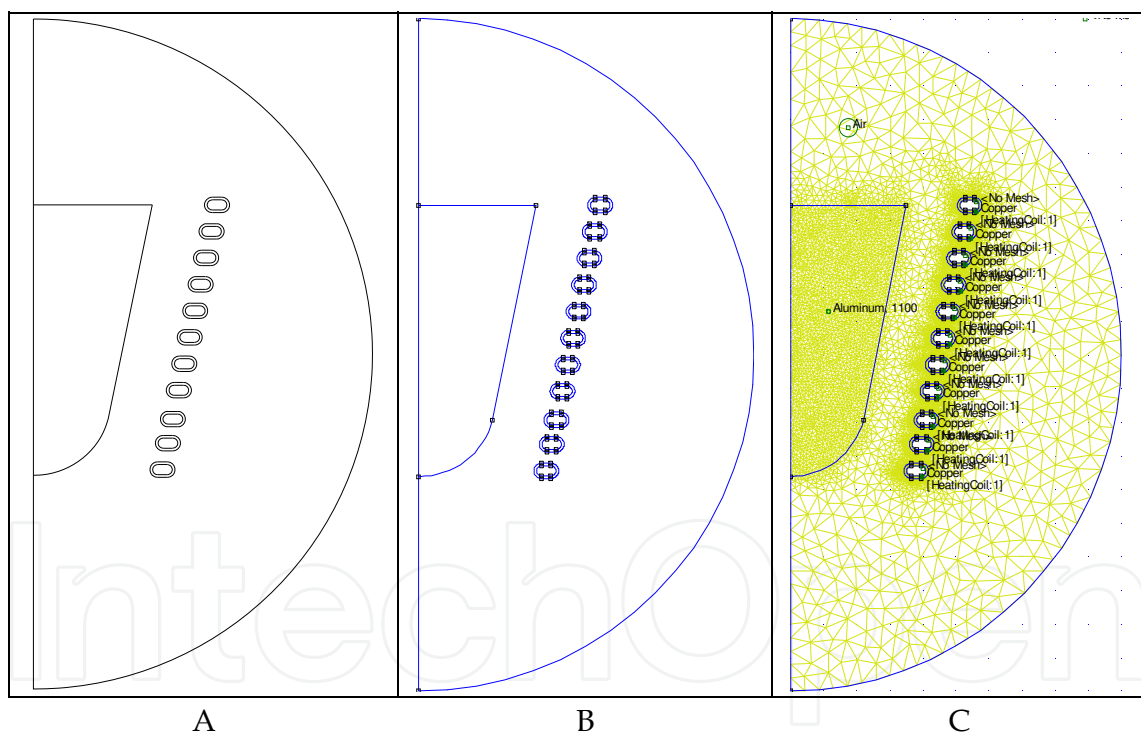


Fig. 4. A: CAD's drawing of the heating system, B: FEMM imported, C: Materials Definitions
 Since all the relevant parameters are already defined, it is possible to make a simulation of the heating system. Fig. 6A illustrates the results, showing the current density both in the coil and the load. Fig. 6B shows the same in a detailed view. It can be seen graphically the Skin Effect since the current tends to go to the conductor's surface and Proximity Effect (Martínez & Esteve, 2003) where currents tend to face each other, incrementing then the effective resistance and changing the system's topology, which means a change in the inductance.

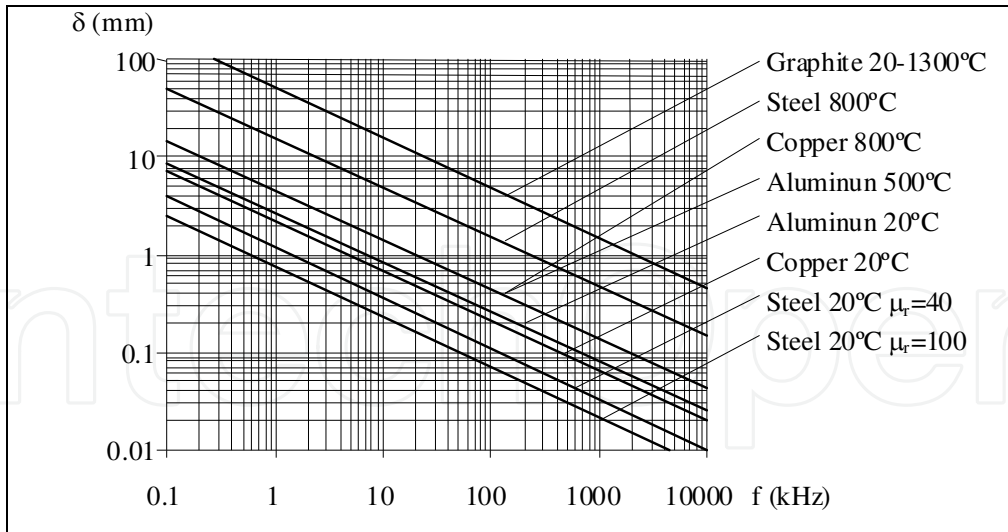


Fig. 5. Penetration deep against frequency for different materials

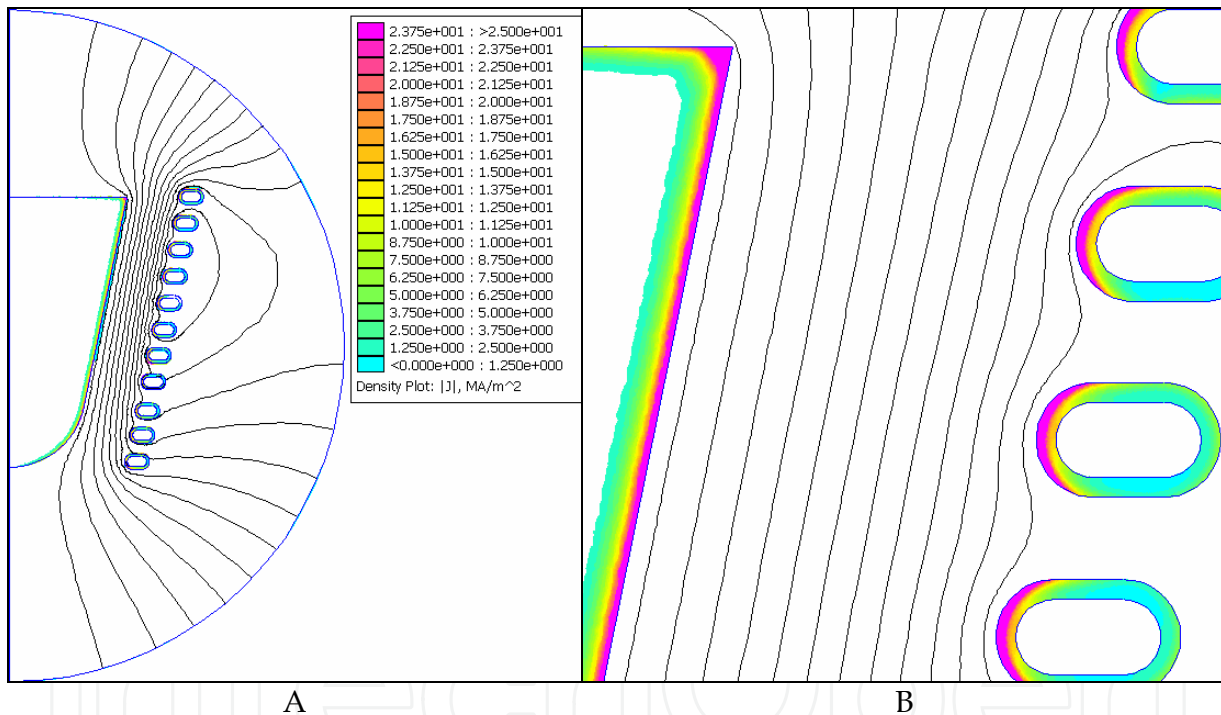


Fig. 6. A: Current density simulation at 40 kHz, B: Load and coil details

Using FEMM postprocessor facility is possible to obtain the parameters needed. With the command *View->Circuits Props* a window pops up with the information shown in Fig. 7. The line “Voltage/Current = 0.0307749+I*1.27647 Ohms” directly gives the values or $R_p+R'_s$ and $L_p-L'_s$, according equations (8) and (9).

$$R_p + R'_s = 0,0307749\Omega \cong 30,7m\Omega \tag{8}$$

$$L_p - L'_s = \frac{1,27647j}{j\omega} = \frac{1,27647j}{2\pi \cdot 40000j} = 5,0789 \cdot 10^{-6}H \cong 5,08\mu H \tag{9}$$

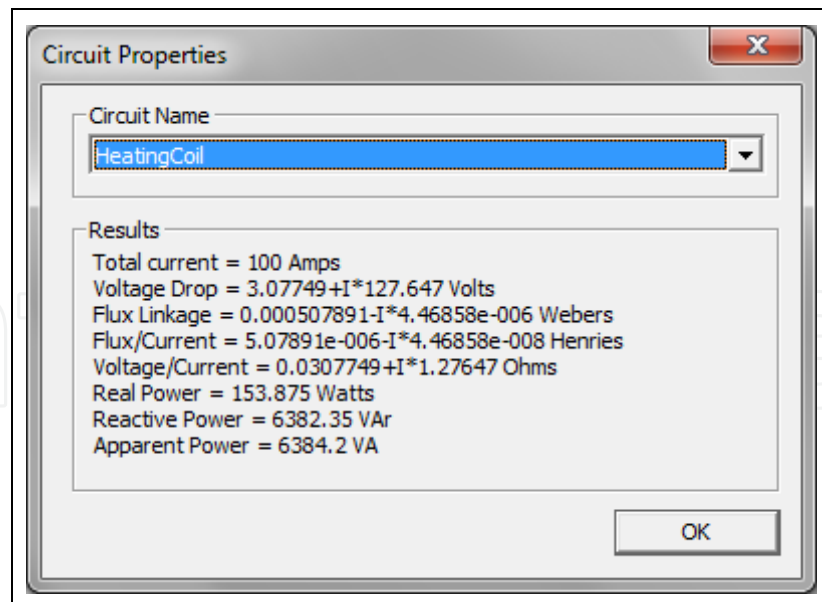


Fig. 7. Heating coil-load circuit properties

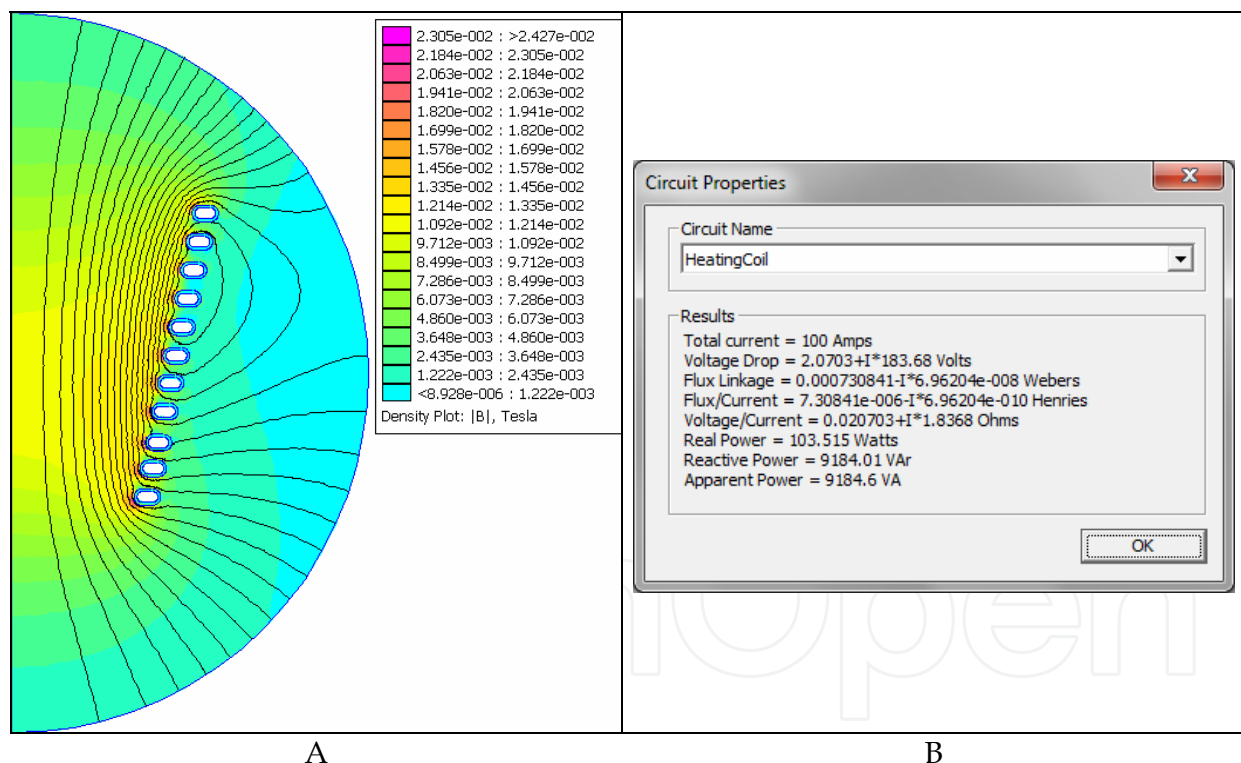


Fig. 8. A: Heating coil only simulation, B: Heating coil circuit properties

Making another simulation eliminating the aluminum load from the FEMM entry data (Fig. 8A), either by deleting or redefining it as “no mesh” will provide the numerical data shown in Fig. 8B.

Repeating the calculation done before

$$R_p = 0,020703\Omega \cong 20,7m\Omega \quad (10)$$

$$L_p = \frac{1,8368j}{2\pi \cdot 40000j} = 7,30839 \cdot 10^{-6} H \cong 7,31 \mu H \quad (11)$$

Now it is possible to obtain the values for R'_s and L'_s . Both are given in equation (12) and (13).

$$R'_s \cong 30,7 m\Omega - 20,7 m\Omega = 10 m\Omega \quad (12)$$

$$L'_s \cong 7,31 \mu H - 5,08 \mu H = 2,23 \mu H \quad (13)$$

All these values are referred to the primary side of the circuit showed in Fig. 2B, therefore these are directly applicable to the circuit of the Fig. 2C. With this information is possible to check the heating efficiency to have an overall idea about the performance of the heating system. Accordingly to equation (7)

$$\eta_{heat} = \frac{R'_s}{R'_s + R_p} \cdot 100\% = \frac{10}{30,7} \cdot 100\% = 32\% \quad (14)$$

This is a rather low figure. It means that 68% of the heating power is dissipated as losses in the induction coil and only 32% contributes to heating the load. Since the last one cannot be modified, it is possible to design and test some other topologies for the induction coil to improve the efficiency. It is left to the reader, as an exercise, to experiment other coil's configurations.

A prototype for the furnace was made with the dimensions used in the FEMM simulations and its partial assembly is shown in Fig. 9.



Fig. 9. Melting furnace partially assembled

4. Mathematical model for the control loop system

Using the terminology adopted in control engineering, it is necessary to define the "plant". We partially did that by creating the model of the heating system showed in Fig. 2C. To complete it requires defining the feeding circuit topology and control type.

All induction heating systems presents to the power generator a large reactive input which must be compensated either partially or totally. Since the heating coil has an inductive behavior, the compensation is made using specially design capacitors which may be connected to the coil either serially, parallel or in a mixed way.

4.1 Power generator review

There are four basic power topologies to energize an induction heating system and they are closely related to the reactive power compensation. Basically these are LC, both serial and parallel and a combination of them (LLC or LCC). The following paragraphs will show a review of these topologies.

4.1.1 Serial compensation

Fig. 10 shows a serially compensated system, often used in relative small systems (Kamli, M. et al. 1998), (Okuno, M. et al. 1998), (Praveen, M. et al. 1998)

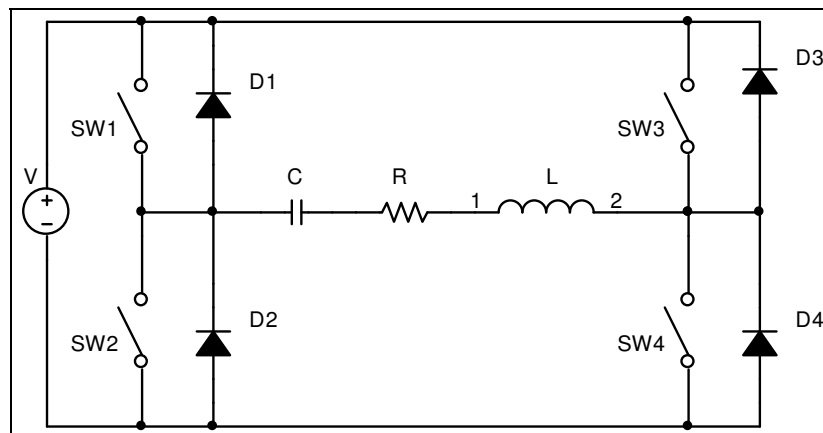


Fig. 10. Serially compensated induction heating system

This topology is fed by a voltage source V which could be fixed or variable. The switches SW1 to SW4 provide the high frequency AC to energize the induction coil L . Typically the coil includes a transformer which is not showed in this circuit, to maintain simplicity. C is the reactive compensation capacitor and D1 to D4 are necessary to maintain a current path when the associated switch is open. It is important to note that the heating coil L represents the total inductance $L_p-L'_s$ and the resistor R is formed by $R_p+R'_s$.

4.1.2 Parallel compensation

Figure 11 shows a system with a parallel type reactive compensator which is usually used in high power systems (Dede et al., 1993a), (Dede et al., 1993b), (Dawson & Jain 1993). This compensator has complementary characteristics to the serial type and must have a current source to feed it instead a voltage source. Again, the heating coil L represents the total inductance $L_p-L'_s$ and the resistor R is formed by $R_p+R'_s$.

4.1.3 Mixed compensation

It is feasible to use a voltage source to power a parallel compensation network (Bonert & Lavers 1999) (Kamli et al.1996) or a current source to supply a serial network (Espí et al. 2000) (Dieckerhoff et al. 1999), but it is necessary then to add an extra inductor or capacitor,

correspondingly. These configurations are shown in Fig. 12A and 12B. R and L have the same meaning than in previous paragraphs.

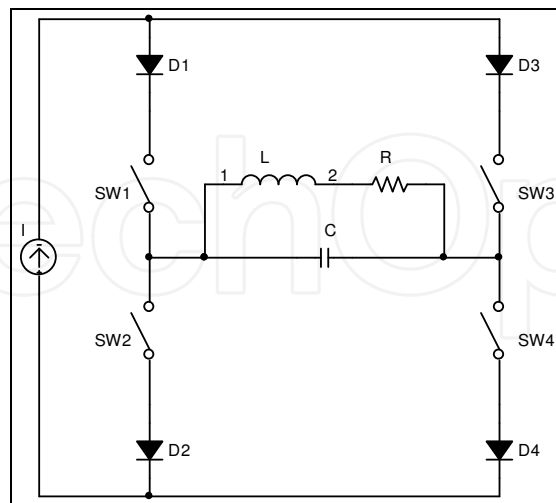


Fig. 11. Parallel compensated induction heating system

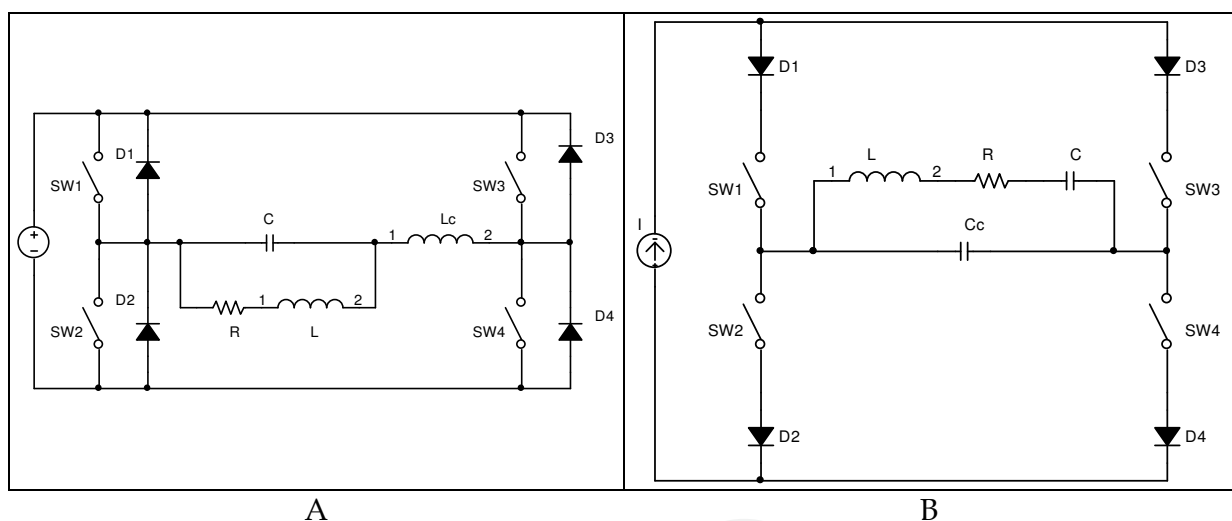


Fig. 12. Mixed compensated induction heating system

4.2 Plant modeling of the compensated induction system

Continuing with the melting oven working example and analyzing the four power topologies, the serial compensation is the best choice for a small system, since it has the simplest topology and the power is supplied by a voltage source which is the most common one.

4.2.1 Response of the serially compensated heating system

The serially compensated circuit shown in Fig. 10 could be simplified to calculate the voltage transfer function, which is one of the easiest variables to control and is directly related to the power injected to the heating system. It is possible also to obtain the current over R but the problems are equivalent. Using Kirchoff Voltage Law in the simplified circuit shown in Fig. 13 and taking the direct Laplace Transform, we have:

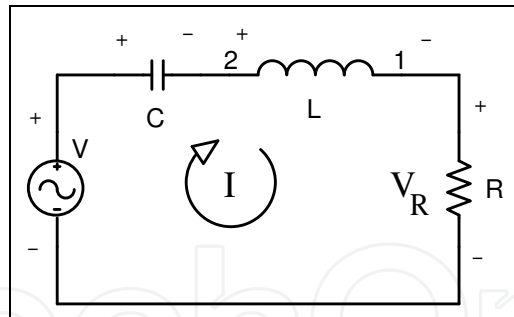


Fig. 13. Simplified serial compensation circuit

$$V(s) - \frac{I(s)}{sC} - sLI(s) - RI(s) = 0 \quad (15)$$

$$V_R(s) = RI(s)$$

Eliminating I from (15)

$$V(s) - \frac{V_R(s)}{sRC} - \frac{sLV_R(s)}{R} - V_R(s) = 0 \quad (16)$$

Placing V_R in function of V

$$V_R(s) = \frac{V(s)}{\left(\frac{1}{sRC} + \frac{sL}{R} + 1 \right)} \quad (17)$$

Arranging the terms and normalizing equation (17)

$$V_R(s) = \frac{sR/L}{s^2 + sR/L + 1/LC} V(s) \quad (18)$$

Finding the denominator's roots of equation (18)

$$s = -\frac{R}{2L} \pm \sqrt{\left(\frac{R}{2L} \right)^2 - \frac{1}{LC}} \quad (19)$$

Normally is desired that the system has an under-damped (oscillatory) response because in most cases the control system locks via a PLL (Phase locked Loop) to this natural frequency, so the roots must be complex and must satisfy the condition:

$$\left(\frac{R}{2L} \right)^2 < \frac{1}{LC} \quad (20)$$

Under this condition, equation (18) could be written as

$$V_R(s) = \frac{sR/L}{(s + (a + j\omega))(s + (a - j\omega))} V(s) = \frac{sR/L}{((s + a)^2 + \omega^2)} V(s) \quad (21)$$

Where

$$a = \frac{R}{2L} \quad y \quad j\omega = \sqrt{\left(\frac{R}{2L}\right)^2 - \frac{1}{LC}} \quad (22)$$

The normalized response of this RLC system to an AC voltage source of magnitude 1 is showed in Fig. 14. The graph was obtained dividing the real part of the network impedance and its modulus.

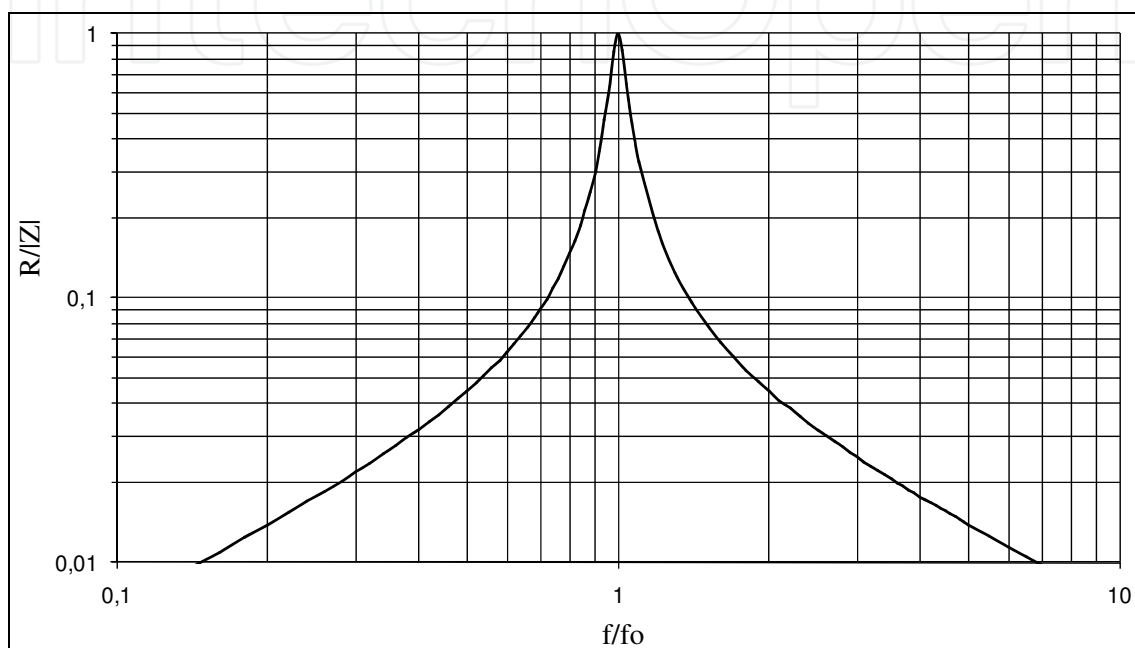


Fig. 14. Normalized response of an RLC system

Figure 14 has also information about which control type could be designed. It is possible to vary the frequency in the region above $f/f_0 > 1$ to have a continuous control of the voltage over R or use a discontinuous control (Hee et al. 1993) or PWM type control (Ogiwara et al. 2001) at exactly the resonance frequency ($f/f_0 = 1$). The zone $f/f_0 < 1$ cannot be used because represent a capacitive-type switching that easily could destroy the switches. The RLC system acts as a filter eliminates the influence of all the harmonics excluding the first one and for this reason, although the commutation of the switches presents a square wave-type signal to the heating system, only the first harmonic matters. For this reason, it is possible to define the source voltage as

$$\begin{aligned} V(t) &= V_i \sin(\omega' t) \\ V(s) &= V_i \frac{\omega'}{(s^2 + \omega'^2)} \end{aligned} \quad (23)$$

Equation (21) could be written now as

$$V_R(s) = \frac{sR/L}{((s+a)^2 + \omega^2)} \cdot V_i \frac{\omega'}{(s^2 + \omega'^2)} = V_i \frac{R}{L} \frac{s\omega'}{((s+a)^2 + \omega^2)(s^2 + \omega'^2)} \quad (24)$$

Where V_i corresponds to the peak voltage of the source, $R = R_p + R'_s$ and $L = L_p - L'_s$. Equation (24) represents the Laplace Transform of the voltage over resistance R and it will be used as the system variable to control the heat over the load. The same procedure could be realized over the other three compensation topologies explained before and are left to the readers as exercises.

4.2.2 Defining the control system

The heat needed to treat any metal by induction has a linear relation with the power injected to the load. In our example it is necessary to melt aluminum and until now it has been developed the dependence of the voltage over the aluminum load in function of parameters extracted from the physical system and the excitation voltage V_i . Now it is necessary to obtain the relation between voltage and power over the resistance R , which is given by

$$W = \frac{V_{RMS}^2}{R} = \frac{V_{Pk}^2}{2R} \quad (25)$$

The chosen control for the working example is discontinuous delta at the resonance frequency ($f/f_0=1$ therefore $\omega=\omega'$) for the reason that it has the capacity of zero switching losses because they are made exactly when the current trough the switches is zero. Since the power is directly related to the capacity of heating the load, the control loop will be a linear one if the control variable is power. Under these conditions, equation (24) could be written as

$$V_R(s) = V_i \frac{R}{L} \frac{s\omega}{((s+a)^2 + \omega^2)(s^2 + \omega^2)} \quad (26)$$

Doing the partial fractions expansion of 26 and taking its Laplace inverse transform

$$V_R(t) = V_i \frac{R}{L} \frac{1}{(a^2 + 4\omega^2)} \left[(1 - \omega e^{-at}) \cos(\omega t) + \frac{2\omega^2 - (a^2 + 2\omega^2)e^{-at}}{a} \text{sen}(\omega t) \right] \quad (27)$$

Since $2a=R/L$, (27) may be written as

$$V_R(t) = V_i \frac{2}{(a^2 + 4\omega^2)} \left[a(1 - \omega e^{-at}) \cos(\omega t) + \text{sen}(\omega t)(2\omega^2 - (a^2 + 2\omega^2)e^{-at}) \right] \quad (28)$$

According (25) the power is proportional to the square of the peak voltage, which could be obtained dropping the oscillatory terms of (28) and taking its value squared. This is equivalent to obtain the envelope of (28). Equation (29) shows this envelope function.

$$V_R(t) = V_i \frac{2}{(a^2 + 4\omega^2)} \left[a(1 - \omega e^{-at}) + 2\omega^2 - (a^2 + 2\omega^2)e^{-at} \right] \quad (29)$$

Arranging the terms of (29) and factorizing it

$$V_R(t) = V_i \frac{2(a + 2\omega^2)}{(a^2 + 4\omega^2)} \left[1 - \frac{(a^2 + a\omega + 2\omega^2)}{(a + 2\omega^2)} e^{-at} \right] = V_i K_1 (1 - K_2 e^{-at}) \quad (30)$$

With

$$K_1 = \frac{2(a + 2\omega^2)}{(a^2 + 4\omega^2)} \quad y \quad K_2 = \frac{(a^2 + a\omega + 2\omega^2)}{(a + 2\omega^2)} \quad (31)$$

It could be conclude from (30) that if the heating system, which natural frequency is ω , is excited with a function $\sin(\omega t)u(t)$, its envelope evolves as a first order system. Figure 15 presents the evaluation of (28) and (30) and shows effectively the relation between the peak voltage and the envelope function as well as its variation in time.

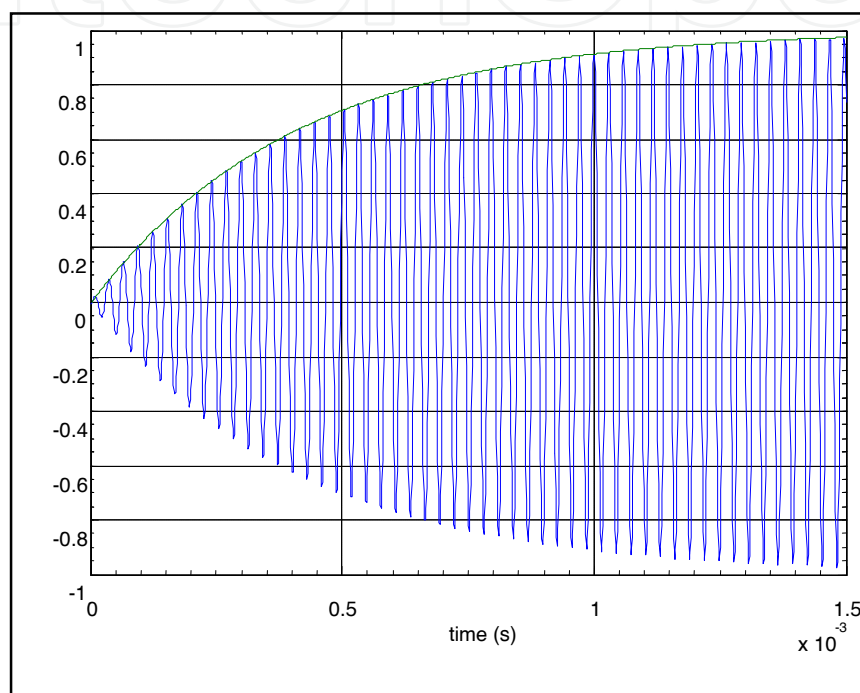


Fig. 15. Normalized response of an RLC system to a resonant excitation

Our interest is obtaining the power over the heating system, so, replacing (30) in (29)

$$W(t) = \frac{V_R^2(t)}{2R_T} = \frac{V_i^2}{2R_T} K_1^2 (1 - K_2 e^{-at})^2 = \frac{V_i^2}{2R_T} K_1^2 (1 - 2K_2 e^{-at} + K_2 e^{-2at}) \quad (32)$$

The control system theory normally requires that the control variable should be represented in the Laplace field, therefore taking the Laplace transform of (32)

$$W(s) = \frac{V_i^2}{2R_T} K_1^2 \left(\frac{1}{s} - \frac{2K_2}{s+a} + \frac{K_2}{s+2a} \right) \quad (33)$$

Expanding (33)

$$W(s) = \frac{V_i^2}{2R_T} K_1^2 \left(\frac{(K_2^2 - 2K_2 + 1)s^2 + (3 - 4K_2 + K_2^2)as + 2a^2}{s^3 + 3as^2 + 2a^2s} \right) \quad (34)$$

Now (34) represents the power over the load as a response to a step $\frac{V_i^2}{2R_T}u(s)$, or

$$W(s) = H(s)u(s) \quad (35)$$

Where $H(s)$ is the plant's transfer function and $u(s)=1/s$ is the transform of the step function $u(t)$, consequently

$$sW(s) = H(s) = \frac{V_i^2}{2R_T} K_1^2 \left(\frac{(K_2^2 - 2K_2 + 1)s^2 + (3 - 4K_2 + K_2^2)as + 2a^2}{s^2 + 3as + 2a^2} \right) \quad (36)$$

Figure 16 shows the response of the plant's transfer function $H(s)$ to a value 1 step. This transfer function contains the system information needed to design the control strategy. The procedure to tune this plant will be developed in the next paragraph.

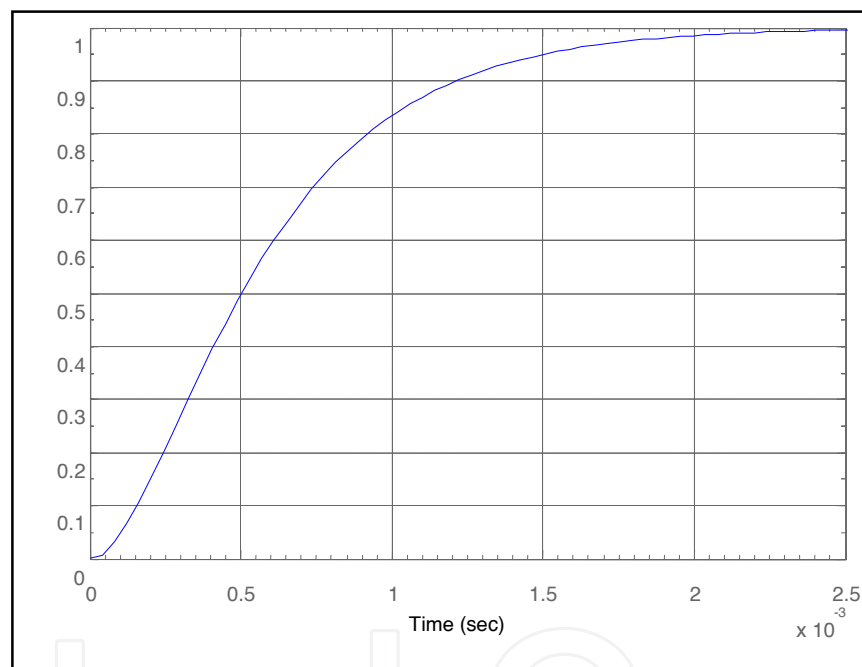


Fig. 16. Step response of the transfer function to a unitary step

It has to be mentioned that all the evaluations were made using MATLAB® (www.matlab.com), but it is possible to do the same using SciLAB (www.scilab.org) or Octave (<http://octave.sourceforge.net/>), which are free software.

5. Control loop tuning using numerical computational tools

Feedback is the standard control topology systematically used in hundred of thousand control systems, from a simple DC power supply to the navigational system of a jet. It is based in taking a sample of the system's output; compare it with a set point and correct the output according this difference. Although an in deep review of the control theory is beyond the scope of this book, there are several books (Ogata 1990) that treat very well this topic. Henceforth, all the calculations are made in MATLAB® using the Control System Toolbox.

It has been already decided that the control variable for the working example is power, but it is necessary to reiterate that it is possible to control other variables like material's temperature. The procedure is the same than the one shown in the example.

5.1 System description

Figure 17 shows the building blocks of the DELTA control loop for the working example induction furnace. Its meaning is explained below.

- Wref: Power set-point
- We: Power error
- Wf: Feedback signal
- Wo: Load Power
- Comparator and FlipFlop: Synchronous Delta generator
- Power Stage: Power Switches, Load Network and Power Supply
- PID: Compensation network
- Sensor: Real Power measurement system

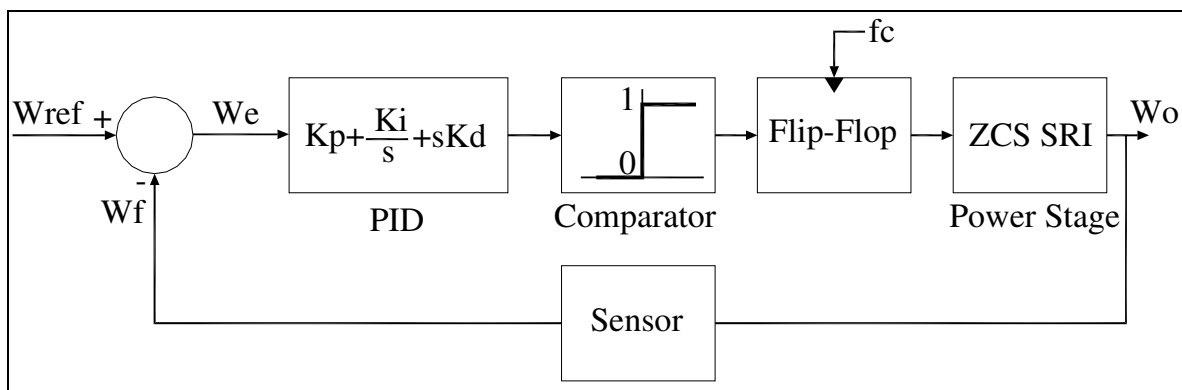


Fig. 17. Block diagram of the closed loop induction system.

Each block has its own properties that contribute to the system response, however, the most important are the Coil-Load Network, the Sensor and the PID because the others blocks only contributes with a scaling factor that can be included in the total response as constants. The coil-load transfer function is already defined, so it remains to obtain the sensor and the PID (Proportional-Integral-Differential compensation network).

5.1.1 Power stage model

As shown in Fig. 17, the PID compensation network output feed a comparator which has a binary output given by (37)

$$Output = \begin{cases} 0 & \text{if } PID < 0 \\ 1 & \text{if } PID > 0 \end{cases} \quad (37)$$

This state is stored in a flip-flop with the zero-crossing current of the load as its synchronous clock, maintaining then the permanent resonant state of the system. The output of the flip-flop manages a driver that activates the high power switches. This conform the Delta Modulator and function in its average behavior as a method to regulate the output power, so it do not contribute to the shape of the transfer function.

The terms a and ω of equation (36) are evaluated using the FEMM obtained parameters shown in equations (10) to (13) and using the formulas for K_1 and K_2 given in (31). The capacitor C used in the heating network to place the system in resonance has a nominal value of 2,7 μF . Equation (38) present the final numerical evaluation of the power transfer function and includes all the constants given by the power supply and coupling transformer.

$$H_{Load}(s) = \frac{0,3177s^2 + 2,695 \cdot 10^5 s + 1,150 \cdot 10^{11}}{s^2 + 7361s + 1,204 \cdot 10^7} \quad (38)$$

5.1.2 Sensor model

Figure 18 shows the heating coil simplified topology. It could be stated that the power is obtained multiplying the instantaneous voltage and current. This multiplication gives a value that differs from the instantaneous power value only by a scale factor.

As was affirmed, the heating coil-load system could be visualized as a serially connected inductor and resistor as is shown in Fig. 18. The current trough L has a sinusoidal form.

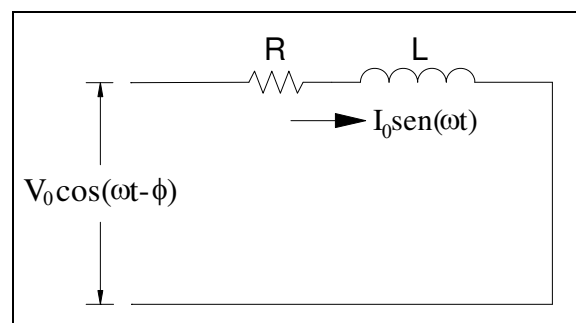


Fig. 18. Induction coil and load model.

The phasor relationships came from the fact

$$V_L = L \frac{di}{dt} = LI_0 \frac{d}{dt} \text{sen}(\omega t) = LI_0 \cos(\omega t) \quad (39)$$

But accordingly the Kirchoff Voltage Law

$$V = V_L + V_R = LI_0 \cos(\omega t) + RI_0 \text{sen}(\omega t) = V_0 \cos(\omega t - \phi) \quad (40)$$

Now, the power over the heating system is VI , then

$$W = VI = V_0 I_0 \text{sen}(\omega t) \cos(\omega t - \phi) \quad (41)$$

By trigonometric identities

$$W = \frac{V_0 I_0}{2} \text{sen}(2\omega t - \phi) + \frac{V_0 I_0}{2} \text{sen}(\phi) \quad (42)$$

Equation (42) shows that the power signal has to components; one is oscillatory with a frequency double than the original while the other is a constant component that depends only from the phase difference ϕ between voltage and current. For the inductive behavior of

the system ϕ is small so $\sin(\phi)$ could be approximated to ϕ . After passing W through a low-pass filter (42) gives

$$\bar{W} = \frac{V_0 I_0}{2} \sin(\phi) \approx \frac{V_0 I_0}{2} \phi \quad (43)$$

Figure 19 shows the block diagram needed to obtain a signal proportional to the power injected into the load

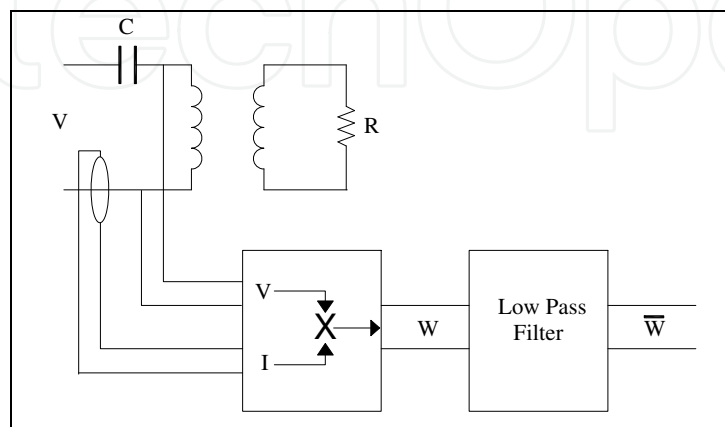


Fig. 19. Block diagram of the Power Sensor.

The Low Pass Filter is somewhat critical because it must have simultaneously a low line delay, a high attenuation and a fast response. As a compromise, it was chosen a fourth order Bessel low pass filter with a cut-off frequency of 5kHz, that gives a maximum response time of 200 μ s, which is sufficient to maintain the parameters of the semiconductor well within its maximums for this particular circuit. The filter is showed in Fig. 20 and was designed using a free program supplied by Texas Instruments (Texas Instrument 2004)

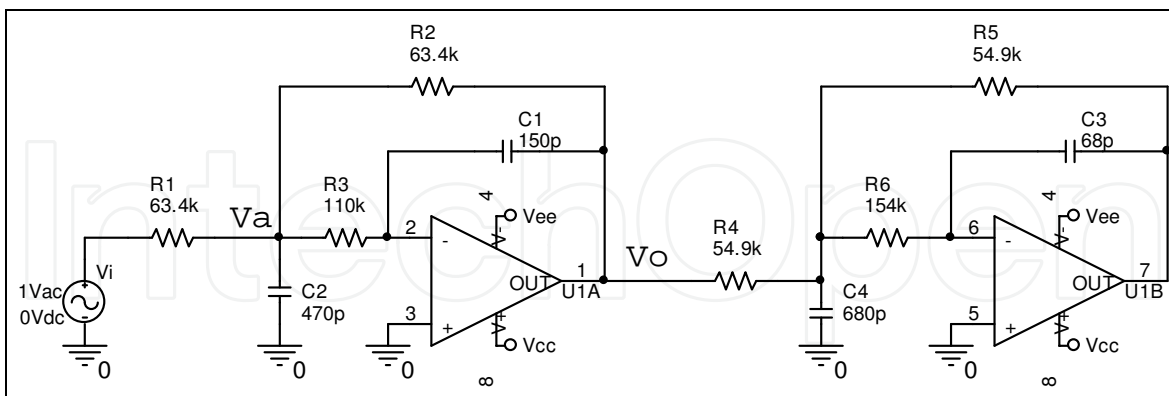


Fig. 20. Fourth order Bessel low pass filter.

It is necessary to obtain now the filter's transfer function to include it in the control loop. Using operational amplifier circuit theory it could be stated

$$\frac{V_i - V_a}{R_1} - \frac{V_a}{\frac{1}{sC_2}} - \frac{V_a}{R_3} - \frac{V_a - V_O}{R_2} = 0 \quad (44)$$

$$\frac{V_a}{R_3} = \frac{V_a - V_O}{\frac{1}{sC_1}} \quad (45)$$

V_a is obtained from 45

$$V_a = -\frac{V_O s R_3 C_1}{1 - s R_3 C_1} \quad (46)$$

And from 44 is obtained V_i

$$V_i = V_a R_1 \left(\frac{R_1 R_2 + R_1 R_3 + R_2 R_3 + s R_1 R_2 R_3 C_2}{R_1 R_2 R_3} \right) - \frac{R_1 V_O}{R_2} \quad (47)$$

Substituting 46 in 47

$$V_i = -\frac{V_O s R_3 C_1}{1 - s R_3 C_1} \left(\frac{R_1 R_2 + R_1 R_3 + R_2 R_3 + s R_1 R_2 R_3 C_2}{R_2 R_3} \right) - \frac{R_1 V_O}{R_2} \quad (48)$$

Simplifying and obtaining common factor V_O

$$\frac{V_i}{V_O} = - \left[\frac{(R_1 R_2 + R_1 R_3 + R_2 R_3 + s R_1 R_2 R_3 C_2) s C_1}{(1 - s R_3 C_1) R_2} + \frac{R_1}{R_2} \right] \quad (49)$$

Adding the fractions and inverting

$$\left(\frac{V_O}{V_i} \right)_1 = - \left[\frac{(1 - s R_3 C_1) R_2}{(R_1 R_2 + R_1 R_3 + R_2 R_3 + s R_1 R_2 R_3 C_2) s C_1 + (1 - s R_3 C_1) R_1} \right] \quad (50)$$

The form of the gain of the second stage is identical to the first one, so it could be inferred directly its transfer function

$$\left(\frac{V_O}{V_i} \right)_2 = - \left[\frac{(1 - s R_6 C_3) R_5}{(R_4 R_5 + R_4 R_6 + R_5 R_6 + s R_4 R_5 R_6 C_4) s C_3 + (1 - s R_6 C_3) R_4} \right] \quad (51)$$

The subscripts of (50) and (51) are referred to the particular filter stage. The complete filter's transfer function was evaluated as

$$\left(\frac{V_O}{V_i} \right)_T = \left[\frac{0,6014 s^2 - 9,388 \cdot 10^4 s + 3,481 \cdot 10^9}{1,020 \cdot 10^{-9} s^4 + 1,292 \cdot 10^{-4} s^3 + 7,766 s^2 + 2,436 \cdot 10^5 s + 3,481 \cdot 10^9} \right] \quad (52)$$

The final transfer function of the power sensor is obtained by multiplying the sensor's transfer function by the filter's transfer functions and was evaluated using the MATLAB symbolic facility. It is represented by equation (55)

$$\bar{W}(s) = H_{Sens}(s) = \frac{3,868 \cdot 10^{-4} s^2 - 135,1 s + 6,766 \cdot 10^6}{5,736 \cdot 10^{-10} s^4 + 1,046 \cdot 10^{-4} s^3 + 5,801 s^2 + 1,884 \cdot 10^5 s + 1,433 \cdot 10^9} \quad (53)$$

5.1.3 PID network model

The PID is a classical analog topology (Ogata 1990) showed in figure 21 and represented mathematically by (54).

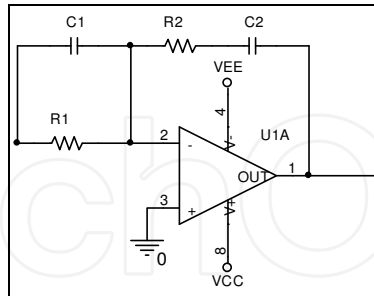


Fig. 21. PID Compensation Network.

$$\frac{V_o(s)}{V_i(s)} = \frac{(sR_2C_2 + 1)(sR_1C_1 + 1)}{sR_1C_2} \quad (54)$$

For the moment, these values are left free. These will be fixed when the system will be tuned using a closed-loop simulator in MATLAB®.

5.2 Tuning the system

Once were determined all the components that shapes the system's transfer function, the remaining task is closing the loop. This will be made using the SISOTOOL (Control 2006) from MATLAB, which permits to visualize the open loop behavior and change the poles and zeroes of the PID compensation network, until a stable configuration could be reach.

Figure 22 shows the system's open loop pole-zero diagrams, as well as the Bode Plot, showing that the system is unstable.

After manipulate the pole-zeroes scheme of the PID network, which is an interactive process, a good result was obtained using the values shown in (55)

$$H_{PID}(s) = 100 \frac{(0,00039s + 1)(0,00022s + 1)}{s} = \frac{(sR_2C_2 + 1)(sR_1C_1 + 1)}{sR_1C_2} \quad (55)$$

Stating one component value, for example for R_1 , the others automatically are fixed, so let $R_1=100k\Omega$, then

$$\begin{aligned} R_1 \cdot C_2 &= 0,01 = 1 \cdot 10^5 \cdot C_2 \Rightarrow C_2 = 0,1\mu F \\ R_2 \cdot C_2 &= 0,00039 = 0,1 \cdot 10^{-6} \cdot R_2 \Rightarrow R_2 = 3,9k\Omega \\ R_1 \cdot C_1 &= 0,00022 = \cdot 10^5 \cdot C_1 \Rightarrow C_1 = 2,2nF \end{aligned} \quad (56)$$

Placing these values on the PID compensating network and then simulates it on SISOTOOL, gives the result shown in Fig. 23

This behavior fulfills the Nyquist Stability Theorem (Ogata 1990), and gives enough phase and gain margin to maintain the loop stable against variations outside the calculated operational point.

With the values shown in equation (56), it is possible now to close physically the control loop showed in Fig 17 and have the possibility of changing the total power in the system simple adjusting the set point (W_{ref})

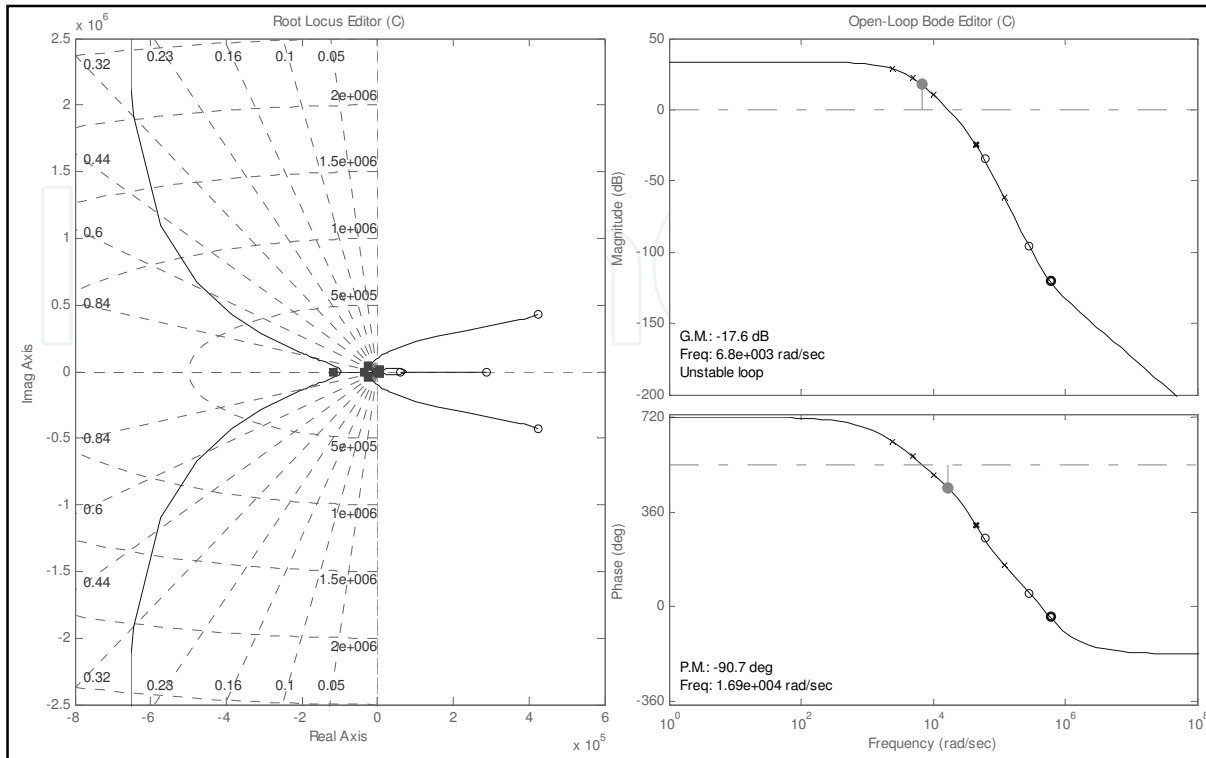


Fig. 22. System's open loop behaviour: Pole-Zeroes Diagram (left); Bode-Plot (right).

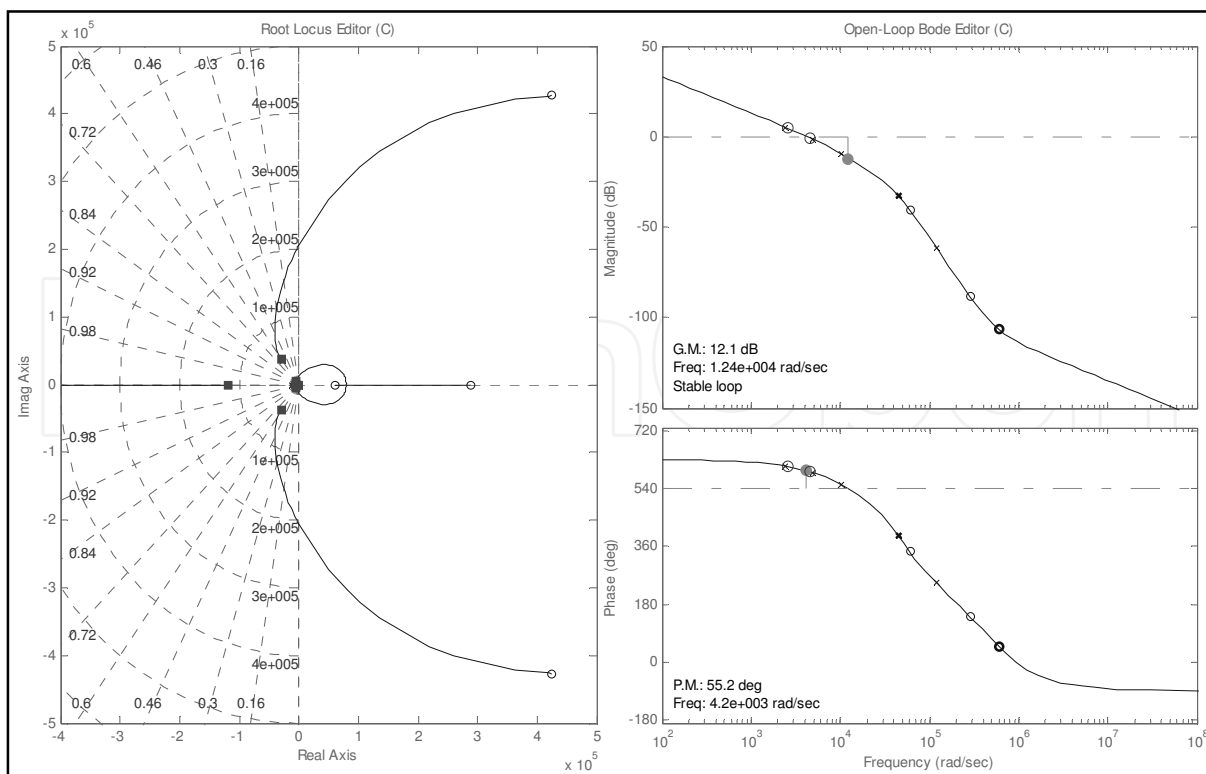


Fig. 23. System's Closed Loop Behavior: Pole-Zeroes Diagram (left); Bode-Plot (right).

6. Results

The results of the working example could be seen in figures 24 and 25. The first correspond to the power output against the voltage on the DC bus for various set points. While the power output is less than the set point is clear the V^2 (parabolic) behavior, but in the moment that the output reaches it, the system maintains a constant power output independently of variations in the bus voltage.

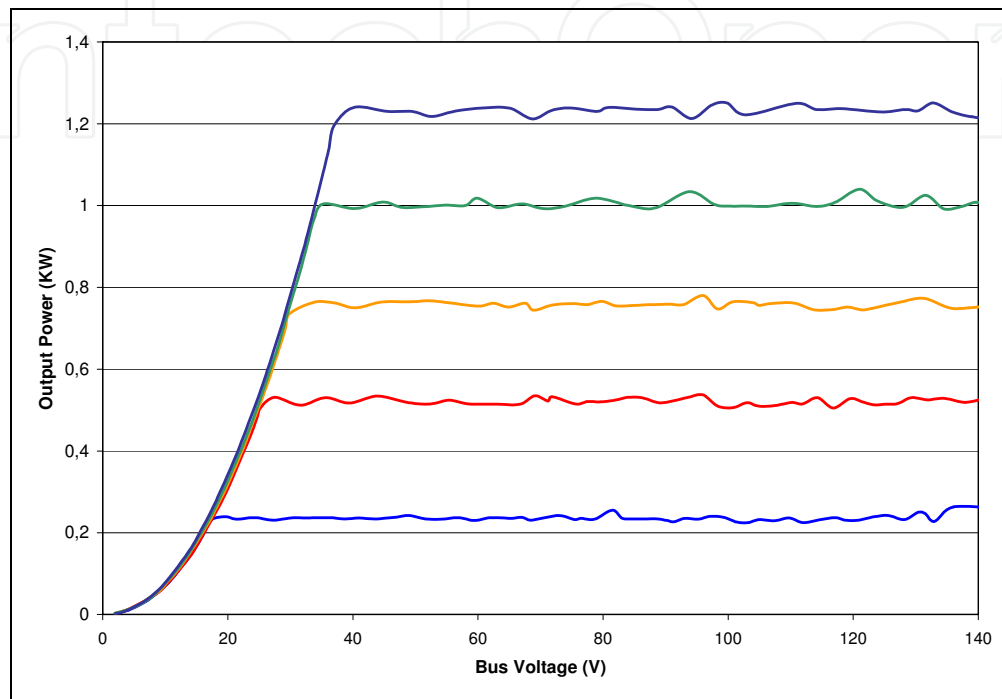


Fig. 24. Output Power response Family vs. Bus voltage

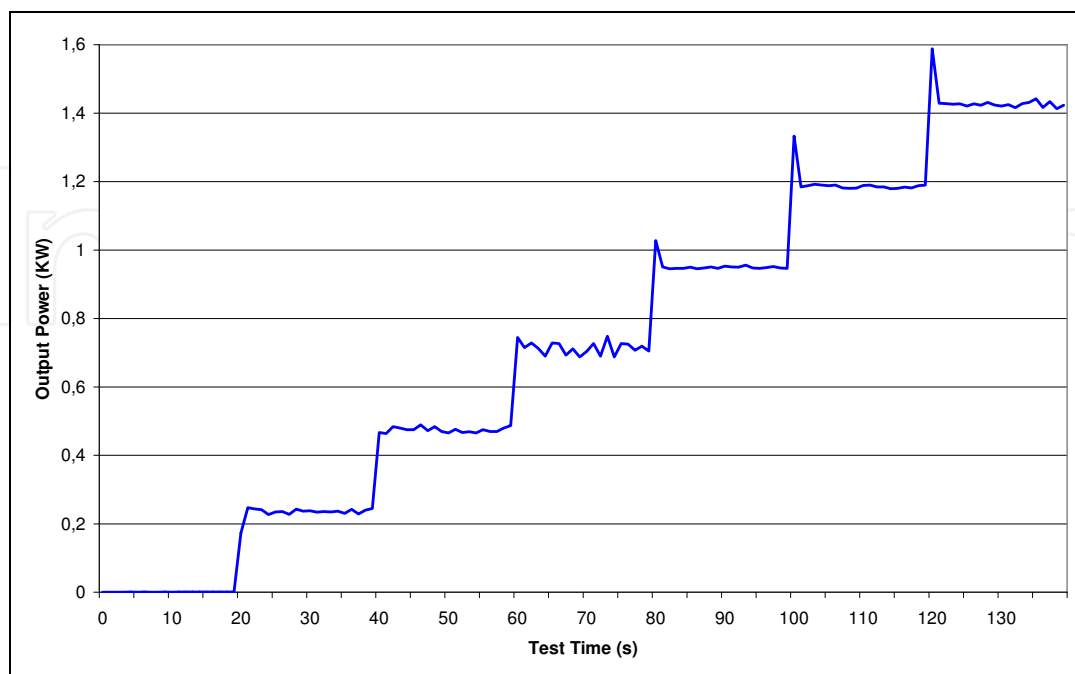


Fig. 25. Output power against set-point

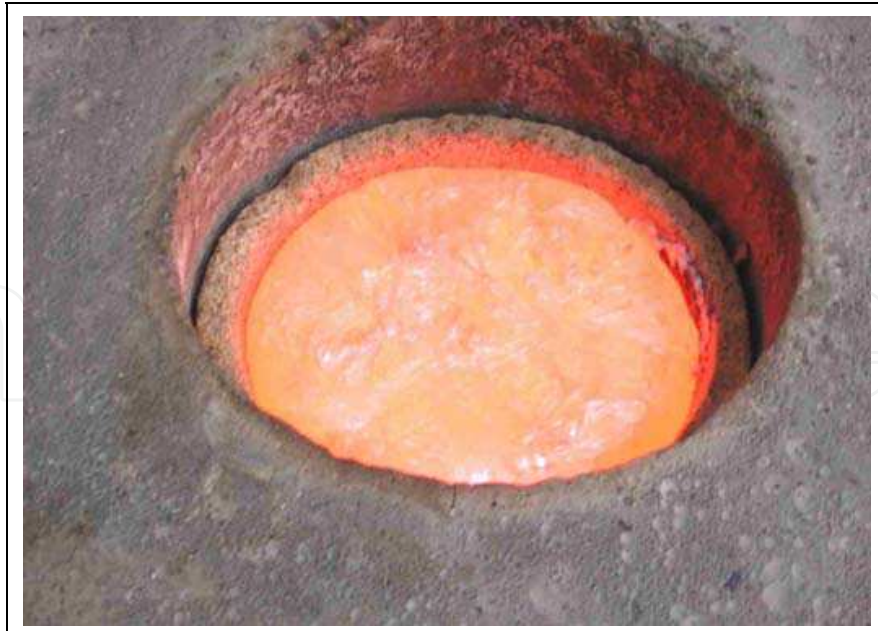


Fig. 26. Melted Aluminum load

Figure 25 shows the output power variation against changes in the set point, for a constant DC bus. It could be seen that the system remains stable when the set point abruptly changes. In the high scale of power, there are small overshoots (approx. 10% of the scale), but it goes back fast to the predetermined level.

Figure 26 shows the operation of the constructed furnace using the techniques developed in this book. 0,5 kg of aluminum load is melted in the crucible at a temperature of 600 C.

7. Conclusion

It was developed a methodology that permit to obtain a precise mathematical model of the coil-load system for an induction heating device, useful for any heating topology. Since the heating coil-load usually is complicated enough to be calculated in a closed form, a Finite Element Magnetic Method is used to extract the relevant parameters that feed the developed model, so the designer may test easily several configurations of the induction coil in a quick way without the need of building any physical device.

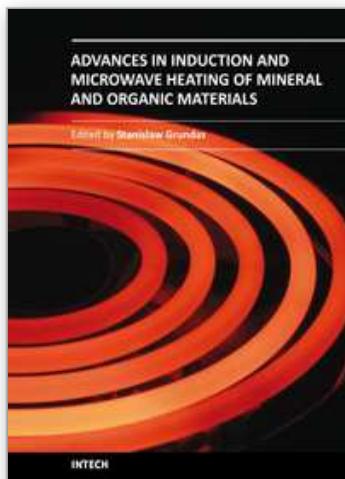
Once the heating device is defined and its parameters are extracted, using the techniques developed it is possible to obtain the transfer functions of the compounds blocks for the control system and using ready available simulation tools, adjust the overall system's behavior without the need of use error-and-trial method that could easily destroy the power semiconductors in a resonant system.

It was designed a small prototype as a working example applying the techniques illustrated in the book. This prototype was built and tested showing the correctness of the principles developed.

8. References

- Bonert, R.; Lavers, J.D. (1994), *Simple starting scheme for a parallel resonance inverter for induction heating*, Power Electronics, IEEE Transactions on, Volume: 9 Issue: 3, May 1994, pp: 281-287
- Control (2006) *Control System Toolbox*, The Mathworks, 18Feb2006
<http://www.mathworks.com/products/control/>

- Curtis F., W. (1950). *High-Frequency Induction Heating*, McGraw-Hill, New York, USA
- Dawson, F.P.; Jain, P. (1993), *A comparison of load commutated inverter systems for induction heating and melting applications*, Power Electronics, IEEE Transactions on, Volume: 6 Issue: 3, July 1991, pp: 430-441
- Dede, E.J.; Esteve, V.; Garcia, J.; Navarro, A.E.; Maset, E.; Sanchis, E. (1993b), *Analysis of losses and thermal design of high-power, high-frequency resonant current fed inverters for induction heating*, Industrial Electronics, Control, and Instrumentation, 1993. Proceedings of the IECON'93., International Conference on, 1993, pp: 1046-1051 vol.2
- Dede, E.J.; Jordan, J.; Esteve, V.; Gonzalez, J.V.; Ramirez, D. (1993a) *Design considerations for induction heating current-fed inverters with IGBT's working at 100 kHz*, Applied Power Electronics Conference and Exposition, 1993. APEC '93, Conference Proceedings 1993, Eighth Annual, 1993, pp: 679 -685
- Dieckerhoff, S.; Ruan, M.J.; De Doncker, R.W. (1999) *Design of an IGBT-based LCL-resonant inverter for high-frequency induction heating*, Industry Applications Conference, 1999. Thirty-Fourth IAS Annual Meeting Conference Record of the 1999 IEEE, Volume: 3, 1999, pp: 2039-2045 vol.3
- Espi, J.M.; Navarro, A.E.; Maicas, J.; Ejea, J.; Casans, S. (2000) *Control circuit design of the L-LC resonant inverter for induction heating*, Power Electronics Specialists Conference, 2000. PESC 00. 2000 IEEE 31st Annual, Volume: 3, 2000, pp: 1430 -1435 vol.3
- Hee Wook Ahn; Byeong Rim Jo; Myung Joong Youn (1993) *Improved performance current regulated delta modulator in series resonant inverter for induction heating application*, Industrial Electronics, Control, and Instrumentation, 1993. Proceedings of the IECON'93., International Conference on, 1993, pp: 857-862 vol.2
- Kamli, M.; Yamamoto, S.; Abe, M. (1996) "A 50-150 KHz Half Bridge Inverter for induction Heating Applications", IEEE Transactions on Industrial Electronics, Vol. 43, No. 1, February 1996, pp: 163-172
- Kamli, M.; Yamamoto, S.; Abe, M. (1996) *A 50-150 KHz Half Bridge Inverter for induction Heating Applications*, IEEE Transactions on Industrial Electronics, Vol. 43, No. 1, February 1996, pp: 163-172.
- Marion, J.; Heald, M. (1980). *Classical Electromagnetic Radiation, Second Edition*, pp 150-156, Academic Press, New York, USA.
- Martínez, J; Esteve, V. (2003) *Inversores Resonantes Serie para Calentamiento por Inducción, Primera Edición*, Pág. 9, Editorial Moliner-40, Valencia, 2003, España
- Meeker D. C. (2009), *Finite Element Method Magnetics, Version 4.2 (02Nov2009 Build)*, <http://www.femm.info/wiki/Documentation/>
- Ogata, K. (1990) *Modern Control Engineering Second Edition*, Prentice-Hall International, Englewood Cliffs, N.J., USA, pp 536-606, 1990
- Ogiwara, H.; Gamage, L.; Nakaoka, M. (2001) *Quasiresonant soft switching PWM voltage-fed high frequency inverter using SIT for induction heating applications*, IEE proceedings for electronic power applications, Vol. 148 . 5, Septiembre 2001, pp: 385-392.
- Okuno, A.; Kawano, H.; Sun, J.; Kurokawa, M., Kojina, A.; Nakaoka, M. (1998) *Feasible development of soft-switched SIT inverter with load-adaptive frequency-tracking control scheme for induction heating*, IEEE Transactions on Industry Applications, Vol. 34, No. 4, July/August 1998, pp: 713-718.
- Praveen, K.; Espinoza, J.; Dewan, S. (1998) *Self-started voltage-source series-resonant converter for high-power induction heating and melting applications*, IEEE Transactions on Industry Applications, Vol. 34, No. 3, May/June 1998, pp: 518-525.
- Texas Instruments (2004) *FilterPro, Filter Design Application (03May2004 Build)* <http://focus.ti.com/docs/toolsw/folders/print/filterpro.html>.



Advances in Induction and Microwave Heating of Mineral and Organic Materials

Edited by Prof. Stanisław Grudas

ISBN 978-953-307-522-8

Hard cover, 752 pages

Publisher InTech

Published online 14, February, 2011

Published in print edition February, 2011

The book offers comprehensive coverage of the broad range of scientific knowledge in the fields of advances in induction and microwave heating of mineral and organic materials. Beginning with industry application in many areas of practical application to mineral materials and ending with raw materials of agriculture origin the authors, specialists in different scientific area, present their results in the two sections: Section 1-Induction and Microwave Heating of Mineral Materials, and Section 2-Microwave Heating of Organic Materials.

How to reference

In order to correctly reference this scholarly work, feel free to copy and paste the following:

Julio Walter and Gerardo Ceglia (2011). Using Numerical Methods to Design and Control Heating Induction Systems, *Advances in Induction and Microwave Heating of Mineral and Organic Materials*, Prof. Stanisław Grudas (Ed.), ISBN: 978-953-307-522-8, InTech, Available from:

<http://www.intechopen.com/books/advances-in-induction-and-microwave-heating-of-mineral-and-organic-materials/using-numerical-methods-to-design-and-control-heating-induction-systems>

INTECH

open science | open minds

InTech Europe

University Campus STeP Ri
Slavka Krautzeka 83/A
51000 Rijeka, Croatia
Phone: +385 (51) 770 447
Fax: +385 (51) 686 166
www.intechopen.com

InTech China

Unit 405, Office Block, Hotel Equatorial Shanghai
No.65, Yan An Road (West), Shanghai, 200040, China
中国上海市延安西路65号上海国际贵都大饭店办公楼405单元
Phone: +86-21-62489820
Fax: +86-21-62489821

© 2011 The Author(s). Licensee IntechOpen. This chapter is distributed under the terms of the [Creative Commons Attribution-NonCommercial-ShareAlike-3.0 License](#), which permits use, distribution and reproduction for non-commercial purposes, provided the original is properly cited and derivative works building on this content are distributed under the same license.

IntechOpen

IntechOpen